Pharmacological clearance of senescent cells reverses HFpEF hallmarks by decreasing inflammation, endothelial dysfunction and cardiac fibrosis

Elsa Silva
i3S
Inês Tomé
CNC https://orcid.org/0000-0001-8147-1004
Francisco Vasques-Nóvoa
FMUP
Glória Conceição
FMUP
Andreia Silva
i3S
António Barros
FMUP https://orcid.org/0000-0002-9103-5852
António Angélico-Gonçalves
FMUP
Carolina Caetano
Centre for Neuroscience and Cell Biology https://orcid.org/0000-0003-0493-7653
Daniel Sousa
i3S https://orcid.org/0000-0002-2334-4610
Daniela Miranda-Silva
i3S
Nádia Gonçalves
FMUP
Vasco Sampaio-Pinto
i3S
Alexandre Gonçalves
i3S
Adelino Leite-Moreira
FMUP
Inês Falcão-Pires
FMUP

Patrícia Pitrez
CNC https://orcid.org/0000-0002-3116-0723
Perpétua Pinto-do-Ó
i3S
Susana Santos
i3S
Lino Ferreira
CNC
Diana Nascimento (dsn@ineb.up.pt)
ICBAS/i3S/INEB https://orcid.org/0000-0001-6402-4245

Article

Keywords: Aging and Chronic Inflammation, Heart Failure, Cellular Senescence, Endothelial Damage, B-type Natriuretic Peptide Levels, Senolytics

Posted Date: July 6th, 2021

DOI: https://doi.org/10.21203/rs.3.rs-624229/v1

Abstract

Aging and chronic inflammation are associated with the development of heart failure with preserved ejection fraction (HFpEF). However, cellular senescence as a potential mechanistic link between both events and its pathophysiological and therapeutic role were yet unexplored. Here we show that ZSF1-obese rats, a model of cardiometabolic HFpEF, have exacerbated systemic inflammation and endothelial damage compared to ZSF1-lean littermates. In addition, ZSF1-obese rats accumulated immune and endothelial senescent cells in the peripheral blood and myocardium. Accordingly, the frequency of circulating senescent leukocytes associated with markers of disease severity in HFpEF patients. Notably, systemic treatment of ZSF1-obese rats with Navitoclax, a BCL-2 family inhibitor, reduced senescent cell burden, decreased circulating B-type natriuretic peptide levels, and attenuated inflammation, vascular remodeling and cardiac fibrosis. Our findings advance cellular senescence as a key mechanistic pathway leading to HFpEF and provide proof-of-concept evidence that senolytics are a promising treatment for this disease.

Introduction

Aging is a major risk factor for the development of heart failure with preserved ejection fraction (HFpEF), which still carries a poor prognosis, and outcome-modifying treatments are a large unmet clinical need[1]. Age-associated chronic systemic inflammation (*i.e.* inflammaging) heightened by cardiovascular comorbidities, such as diabetes mellitus, hypertension and dyslipidemia, has been suggested as a key driver of cardiac microvascular dysfunction and matrix remodeling, both contributing to increase myocardial stiffness[2]. Accordingly, pharmacological targeting of inflammation provides clinical benefit to patients with high cardiovascular comorbidity load[3,4]. Nevertheless, upstream mechanisms driving inflammation in HFpEF remain poorly understood.

Age-associated accumulation of senescent cells (SCs) is a significant contributor to inflammaging and age-dependent tissue dysfunction[5–7]. SCs promote aging by acquiring a senescence-associated secretory phenotype (SASP)[8] which is pro-inflammatory, pro-fibrotic and may spread the senescence program to neighboring cells[9]. During aging, immune-mediated SCs clearance becomes impaired in part due to age-related changes in the composition and function of immune cell subsets (*i.e.* immunosenescence)[10]. On the other hand, immune cells can also acquire a senescent phenotype, further contributing to the accumulation of SCs in older individuals. A link between endothelial senescence and HFpEF was recently demonstrated in a mouse model of accelerated aging[11]. However, the impact of SCs in the pathophysiology and treatment of HFpEF, in relevant pre-clinical models, remains unexplored.

Based on the hypothesis that cellular senescence may collectively contribute to the development of a systemic deleterious environment in HFpEF, anti-senescence pharmacological strategies may emerge as new therapeutic avenues. Senolytic drugs induce systemic clearance of SCs by promoting targeted apoptosis[12,13]. Among these, Nav (ABT-263), a BCL-2/BCL-XL inhibitor, has shown effectiveness in

diseases marked by vascular remodeling and fibrosis, namely in experimental models of myocardial infarction and HF with reduced ejection fraction[12,14,15].

In the present work, we used obese ZSF1 rats that develop an HFpEF-like phenotype between the 14th and 20th weeks of age[16,17,18] to analyze systemic and cardiac inflammation, the immune system and endothelial dysfunction at disease onset (week 15) and onwards. We then characterized the senescence program of immune, circulating endothelial and cardiac cells. In addition, the association between cell senescence with diagnostic and prognostic markers in HFpEF, such as B-type natriuretic peptide (BNP), was investigated in a patient cohort. Finally, we evaluated the therapeutic effects of the systemic administration of a pharmacological agent to eliminate SCs. The results obtained support that premature aging is a key driver of HFpEF and that senolytics hold promise for its treatment.

Results

Obese ZSF1 rats show alterations in the immune system, inflammaging and endothelial dysfunction

The composition of the immune system in obese ZSF1 (ZSF1-Ob, Ob) and lean ZSF1 rats (ZSF1-Ln, Ln) is relatively unknown. Therefore, peripheral mononuclear blood cells (PBMCs) of ZSF1-Ob and Ln rats were characterized by flow cytometry from week 15 to week 28 following the gating strategy described in Extended Data Fig. 1a. ZSF1-Ob rats showed higher percentage (Fig. 1a-b) and number (Fig. 1e) of myeloid ($CD45R^{-}TCR^{-}CD161a^{-}CD11bc^{+}$) and activated natural killer (NK^{dim}) cells[19] ($TCR^{-}CD161a^{dim}$) as compared to ZSF1-Ln littermates, an effect that increased with aging. In addition, ZSF1-Ob rats showed higher M1/M2 (CD40/CD163) myeloid polarization, indicative of a pro-inflammatory profile (Extended Data Fig. 1b). These alterations were accompanied by a decrease in the percentage of T ($TCR^{+}CD161a^{-}$) and B (CD45R) cells in ZSF1-Ob rats (Fig. 1c-d) whereas some fluctuation in the percentage of NK^{bright} cells, NKT cells and T subpopulations was observed overtime, without a clear trend (Extended Data Fig. 1c-f). This phenotype also extended to main hematopoietic organs such as the spleen, lymph nodes and bone marrow (BM) (Extended Data Fig. 2a-f). Moreover, a decrease in the relative percentage of hematopoietic progenitors (HPC) (Fig. 1f) in BM of ZSF1-Ob rats was accompanied with a higher capacity of these cells to differentiate into the granulocytic-monocytic lineage (Extended Data Fig. 2g-h).

Due to the pro-inflammatory nature of myeloid cells, we further investigated plasma cytokine and chemokine profiles. Our results indicate significantly higher levels of pro-inflammatory cytokines and chemokines in the plasma of ZSF1-Ob than ZSF1-Ln rats such as MIP-1A, IL-18 and IP-10 at week 22 and IL-1α, MIP-1A, IL-6, IL-18, MCP-1 and TNF-α at week 26 (Fig. 1g). We then evaluated the impact of this pro-inflammatory milieu in cardiac endothelial cells, a driver of myocardial dysfunction in HFpEF[2,20]. For this purpose, we exposed human cardiac microvascular endothelial cells (MVECs) to plasma (Fig. 1h) or conditioned medium collected from bone marrow macrophages (CM BM-Mac) (Extended Data Fig. 2i). Remarkably, the plasma of ZSF1-Ob rats was able to activate MVECs, as demonstrated by an increased percentage of $ICAM\text{-}I^{+}$ and $VCAM\text{-}I^{+}$ cells (Fig. 1i). This activation effect was less pronounced in response to CM BM-Mac (Extended Data Fig. 2j). In addition, a higher percentage of activated MVECs were positive

for the conventional apoptotic marker annexin V, indicating that these cells entered in an apoptotic program (Fig. 1j). Strengthening the translational relevance of these findings, human HFpEF patient plasma also induced MVECs activation, as demonstrated by higher percentage of P-selectin^{+} MVECS in response to control patient's plasma (Fig. 1k-l). Of note, circulating endothelial cells (CECs; CD31^{+} CD45^{+}), recognized as markers of endothelial injury[21], were increased in the blood of ZSF1-Ob than of ZSF1-Ln rats from week 18 onwards (Fig. 1m-n). At week 28, the number of CECs in the blood of ZSF1-Ob decreased relatively to week 22 (Fig. 1n), which is likely due to the higher number of apoptotic CECs at week 28 than 22 (Fig. 1o).

Altogether, our results suggest that alterations in the genesis and production of main immune cell populations occur earlier in ZSF1-Ob animals and contribute to the establishment of a systemic deleterious pro-inflammatory environment that promote endothelial alterations.

Hearts from ZSF1-Ob rats show infiltration of immune cells, endothelial dysfunction and fibrosis

The non-cardiomyocytic cellular compartment of ZSF1-Ob and ZSF1-Ln ventricles was characterized by flow cytometry at weeks 22 and 28, according to the gating strategy presented in the Extended Data Fig. 3a. The level of infiltrating immune cells (CD45^{+}) in the heart of ZSF1-Ob rats was higher than ZSF1-Ln at week 22 (Fig. 2a) and was mainly composed of myeloid cells (CD45^{+}CD11bc^{+}) (Fig. 2b). These results were supported by immunofluorescence in myocardial sections, which showed the presence of significantly higher percentage of macrophages (CD68^{+}) in the heart of ZSF1-Ob rats than of ZSF1-Ln animals (Fig. 2c-d). Alongside immune infiltration, endothelial cell activation (ICAM-1^{+} and VCAM-1^{+} cells) was augmented in the hearts of ZSF1-Ob rats (Fig. 2e-f). Of note, a reduction in the frequency of cardiac endothelial cells (CD45^{-}CD31^{+}) was observed in ZSF1-Ob rats from week 22 to 28 (Fig. 2g), resulting in poor microvascular density compared to ZSF1-Ln rats (Fig. 2h-i). Together with these alterations, fibroblasts (CD140a^{+}) frequency was increased in ZSF1-Ob hearts (Fig. 2j), as well as the expression of fibrosis-associated genes in whole heart tissue compared to ZSF1-Ln (Fig. 2k).

Taken together, these findings support that immune infiltration and endothelial activation precede the development of vascular rarefaction and fibrosis in ZSF1-Ob rats.

Senescent phenotype of immune and endothelial cells in ZSF1-Ob rats

PBMCs displayed high activity of senescent-associated beta-galactosidase (SA-β-gal), a classical biomarker of cell senescence[22], which increased significantly with aging in all groups of ZSF1 animals (Fig. 3a). However, SA-β-gal^{+} PBMCs were consistently more abundant in ZSF1-Ob rats since week 15, a life stage in which cardiac dysfunction is at an early phase[23] (Fig. 3a). Monocytes comprised the large majority (75 to 90%) of SA-β-gal^{+} PBMCs, being this percentage higher in ZSF1-Ob rats comparing with ZSF1-Ln animals (Fig. 3b). Consistently with a senescent phenotype, PBMCs of ZSF1-Ob showed higher expression of the senescence marker p21 (Fig. 3c) at weeks 22 and 28, and of senescence associated secretory phenotype (SASP) molecules such as IL-6, IL1-β and TGF-β at week 22, and IL-10, IL-1β, TNF-α

and iNOS at week 28, when compared to ZSF1-Ln rats (Fig. 3d). Moreover, ZSF1-Ob PBMCs displayed up-regulation of the anti-apoptotic molecule BCL-XL at 18 weeks of life (Fig. 3e-f), whereas BCL-2 is down-regulated in all studied time-points (Fig. 3e,g).

CECs present in peripheral blood of ZSF1-Ob (Fig. 3h), as well as cardiac cells isolated from the heart of ZSF1-Ob rats at week 28 (Fig. 3i), showed higher cellular senescence than counterparts collected from ZSF1-Ln rats, as confirmed by SA-β-gal staining. In the heart, SA-β-gal^{+} cells were more abundant in immune and endothelial compartments (Fig. 3j) at 20 and 28 weeks. Importantly, cardiac cells from ZSF1-Ob rats expressed higher levels of senescence markers p21 and p53 at week 28 than ZSF1-Ln rats (Fig. 3k), as well as increased levels of SASP-associated molecules such as MCP1, IL-6 and TGF-β (Fig. 3l). Of note, no differences were found in SA-β-gal levels in cells collected from BM, spleen and subcutaneous fat (Extended Data Fig. 3b-d).

Overall, our results demonstrate the early onset of a cellular senescence program in peripheral blood of ZSF1-Ob animals (at week 15 for immune cells and week 20 for CECs), that extended specifically to the heart (immune and endothelial compartments from week 20 onwards).

Circulating senescent cells associate with cardiac overload surrogates and key drivers of human HFpEF

To assess the translation potential of our findings, we investigated the senescence program in PBMCs collected from HFpEF patients and comorbidity-matched control patients (Extended Data Table 1). Interestingly, no significant association was found between the burden of circulating senescent (SA-β-gal) cells and age. However, despite similar percentage of SCs in both groups (Fig. 4a), higher HFpEF severity (NYHA III) was associated with increased SCs fraction (Fig. 4b). Accordingly, the number of SCs correlated with BNP levels (Fig. 4c) and pulmonary artery systolic pressure (PASP) (Fig. 4d), key analytical and clinical surrogates of cardiac overload, respectively. Of note, clinically relevant biomarkers of inflammation (high-sensitivity C-reactive protein, hsCRP, and monocytosis), glycemia/diabetes control (glycated hemoglobin, HbA1c) and body mass index (BMI) could be found among explanatory variables of SCs variation (Fig. 4e). Altogether, our results suggest that SCs burden is correlated with disease severity and is highly modulated by major risk factors for developing HFpEF.

Nav-treated ZSF1-Ob rats display lower levels of circulating BNP, inflammation and immunosenescence

Previous studies have shown that Nav, a potent small-molecule inhibitor of BCL family, improved the recovery after myocardial infarction[14], as well as inflammation and ejection fraction in a model of HF with reduced EF[12], through systemic elimination of SCs. Therefore, we investigated whether clearance of senescence cells by Nav (*i.e.* by inhibition of the anti-apoptotic pathway BCL-XL upregulated in ZSF1-Ob rats at week 18) (Fig. 3e-f) could alleviate the disease progression in ZSF1-Ob rats. Upon the establishment and characterization of the HFpEF phenotype, 18-week-old ZSF1-Ob rats were treated with Nav (50 mg/Kg/day) or vehicle (DMSO + PEG-300) in a 2-cycle administration regimen, with 2 weeks of interval (Fig. 5a). Remarkably, treatment of ZSF1-Ob rats with Nav decreased systemic inflammation (Fig. 5b) at week 26, reducing the levels of several inflammatory cytokines, and BNP levels at weeks 22

and 26, a marker of cardiac overload and key prognosticator in HF patients[24,25] (Fig. 5c), relative to non-treated ZSF1-Ob rats. Although the Nav treatment in ZSF1-Ob rats had no statistical effect in the body weight and exercise intolerance (Extended Data Table 2), high metabolic risk features such as perirenal fat, hyperglycemia, total cholesterol and circulating urea were alleviated with Nav treatment (Extended Data Table 2). Importantly, at systemic level, Nav treatment decreased the senescence program in PBMCs of ZSF1-Ob rats (week 28), as demonstrated by a decrease in SA-β-gal$^+$ cells (Fig. 5d), in the expression of senescence-related gene p21 and of the SASP molecules TGF-β and iNOS (Fig. 5e), and a tendency to decrease BCL-XL/BAX ratio, suggesting increased apoptosis of senescent PBMCs after Nav treatment (Fig. 5f-g).

Treatment of ZSF1-Ob rats with Nav decreased the percentage of pro-inflammatory cellular orchestrators, particularly myeloid cells (Fig. 5h-i), and increased the percentage of T cells in PBMCs (Fig. 5j), while no differences were detected at the level of B cells (Fig. 5k). In the BM, Nav treatment restored the proportion of myeloid cells, whereas other immune subsets and hematopoietic progenitors were not affected (Extended Data Fig. 4a-d).

Taken together, our results show that Nav promoted clearance of SCs, decreased systemic inflammation and BNP levels, and partially rescued the composition of the immune system.

Treatment of ZSF1-Ob rats with Nav decreased heart cell senescence, fibrosis and endothelial dysfunction

A recent study has shown that Nav is able to improve vascular and myocardial function in aged hearts through the elimination of SCs[1]. However, the therapeutic potential of Nav remains to be determined in the context of HFpEF. Echocardiographic analyses at week 28 confirmed that the Nav treatment in ZSF1-Ob rats did not affect cardiac function (Table 1). ZSF1-Ob rats treated with Nav showed lower levels of SA-β-gal in cardiac cells (Fig. 6a), particularly in immune and endothelial cells, as compared to non-treated ZSF1-Ob rats (Fig. 6b), decreased expression of p21 and BNP (Fig. 6c), reduced SASP markers, namely TGF-β, TNF-α and iNOS (Fig. 6c), and a non-statistical decrease in the percentage of cells with DNA damage (Extended Data Fig. 4e-f).

Next, the impact of Nav treatment in myocardial fibrosis and immune cell infiltration, cardiomyocyte physiology and cardiac endothelial cell number and activation was investigated at week 28. The Nav treatment reduced the frequency of myocardial macrophages (Fig. 6d-e and Extended Data Fig. 4g) and fibroblasts (Fig. 6f), and a decrease in fibrosis as confirmed by picrosirius red staining (Fig. 6g-h and Extended Data Fig. 4h) and fibrosis-associated genes, namely of collagen type 3 and alpha smooth muscle actin (α-SMA) (Fig. 6i). In addition, Nav treatment of ZSF1-Ob rats had no impact in cardiomyocyte hypertrophy (assessed by cross-sectional area), in agreement with the LV mass estimation by echocardiography (Extended Data Figs. 4i-j). The proportion of cardiac endothelial cells was not significantly increased (Fig. 6j) but their activation profile was improved (Fig. 6k), as was the myocardial microvasculature density, assessed by Isolectin B4 (Fig. 6i-m and Extended Data Fig. 4k).

Altogether, our results demonstrate that ZSF1-Ob rats treated with Nav showed decreased cardiac overload, cardiac cell senescence, immunosenescence, fibrosis and endothelial activation.

Treatment of ZSF1-Ob rats with Nav decreased circulating endothelial cells, vascular cell senescence and hypertrophy

We next investigated whether vascular remodelling was extended to the peripheral system, besides the myocardium. Nav treatment abrogated the increase in frequency of CECs in the peripheral blood of ZSF1-Ob rats, when compared to ZSF1-Ln animals (Fig. 7a). Nav treatment also significantly decreased the frequency of SA-β-gal^{+} (Fig. 7b) and Annexin V^{+} cells (Fig. 7c), and reduced p21 levels in the aorta of obese rats (Fig. 7d-e), as confirmed by RNA-ISH analysis. In addition, ZSF1-Ob rats treated with Nav showed decreased cross-sectional area and a trend of lower media wall thickness and larger lumen area, which indicates that the treatment was able to attenuate hypertension-induced vascular remodeling (Fig. 7f-i and Extended Data Fig. 5a). While elastin and collagen content remain unchanged with Nav treatment (Extended Data Figs. 5b-c), a trend for reduced elastin fragmentation was found (Fig. 7j).

In summary, our results demonstrated that Nav treatment of ZSF1-Ob rats restored vascular compartment by decreasing the frequency of SCs in vascular endothelium and ameliorating aortic remodelling.

Discussion

Limited success has been achieved so far in improving HFpEF outcomes[26,27,28]. One of the main difficulties in tackling this problem stems from an incomplete understanding of upstream mechanisms leading to early disease manifestations, including systemic inflammation and endothelial dysfunction, important triggers of structural and functional cardiac alterations. Here, we show that immune dysregulation and accumulation of circulating and myocardial SCs may contribute to the establishment of systemic inflammation and endothelial dysfunction in a pre-clinical animal model of HFpEF. We further show that higher levels of SCs in patients associate with major risk factors and prognosticators in HFpEF, specially with cardiac overload surrogates. Moreover, circulating SCs burden positively associates with hsCRP and HbA1c, important biomarkers of inflammation and glycemic control, whereas a negative correlation was showed for BMI. Curiously, mildly elevated BMI levels are known to be protective regarding mortality in HFpEF (obesity paradox) by mechanisms yet to be clarified[29], but among which senescence can potentially play a role.

Importantly, the treatment of ZSF-1-Ob rats with the senolytic compound Nav decreased the number of SCs, systemic inflammation, endothelial dysfunction and circulating BNP levels, as well as rejuvenated the immune system, decreased cardiac fibrosis and vascular remodeling. These findings support cellular senescence as a likely driver of HFpEF and indicate senolytics as a potential pharmacological alternative for this prevalent syndrome.

Age-associated immune dysfunction and accumulation of SCs in blood and heart is observed at the onset of HFpEF disease. ZSF1-Ob animals display an increase in the frequency and absolute numbers of

circulating myeloid cells, displaying a pro-inflammatory and senescent phenotype, and of mature (NK^{dim}) cells. Similar alterations have been described in HFpEF patients, namely the increase in myocardial tissue macrophage density and number of circulating pro-inflammatory monocytes[30,31]. Herein, alterations in immune subsets of ZSF1 obese rats were accompanied with the emergence of SCs in the immune-myocardium-endothelium axis, while other organs, like fat and spleen, failed to show features of cellular senescence. Although endothelial cell senescence has been previously described in an aging mouse model of HFpEF[11], the existence of a senescence program in HFpEF immune and cardiac cells has not been previously investigated. Our observations of immunosenescence are in line with recent results from single cell transcriptomics showing that altered immune populations also display a senescent profile in the context of aging and infection[32–34]. In fact, activation of the senescence program in immune cells has been implicated in the functional deterioration of multiple organs, including the heart[14,34–36]. For example, senescent macrophages found in subendothelial space at the onset of atherosclerosis drive pathology progression through SASP[34] in atherosclerosis-prone low-density lipoprotein receptor-deficient ($Ldlr^{-/-}$) mice. In ZSF-1-Ob, senescence of immune circulating cells precedes myocardial aging and damage. These finding are in line with the recent data showing that senescent immune cells drive accelerated aging and local tissue damage in multiple organs, including the heart[36].

Despite the known role of inflammation on HFpEF pathophysiology and promising data from trials[3,4], anti-inflammatory therapies have not yet been included in the disease management routine care. Herein, we show that the systemic treatment of a preclinical model of HFpEF with a senolytic drug[37,38] significantly decreased age-related inflammation, endothelial dysfunction, BNP levels and cardiac fibrosis. To the best of our knowledge, this is the first study to use an anti-senescence therapy to treat HFpEF. Nav was selected because it targets the BCL family of proteins, which were found to be dysregulated in ZSF1 obese animals, and has previously shown efficacy in the elimination of SCs from the main systems affected by the senescence program in the ZSF1 obese, *i.e.* the endothelium[39], the hematopoietic system[34,40] and the heart[14]. The selective depletion of SCs stimulated immune recovery towards a physiological and less inflammatory phenotype. A similar outcome has been previously reported following Nav administration to sub-lethally irradiated or normally aged mice, which effectively cleared senescent hematopoietic bone marrow stem cells[40]. Conversely, the bone marrow of ZSF1 obese showed no signs of SCs accumulation, despite having an aged phenotype associated with a myeloid skewing in differentiation.

In summary, our study provides evidence for the etiology of HFpEF indicating that immunosenescence and accumulation of SCs in the immune-myocardium-endothelium axis are major generators of inflammaging and endothelial dysfunction, and offers a proof-of-principle that systemic clearance of SCs attenuates HFpEF phenotype.

Methods

Detailed protocols are also available in Supplementary Information.

Human Samples

Clinical data and peripheral blood samples were obtained from HFpEF and comorbidity-matched control patients at Centro Hospitalar Universitário São João. HFpEF diagnosis followed European Society of Cardiology (ESC) guidelines[41] and Heart Failure Association of the ESC consensus recommendations[42]. In order to control for the confounding effect of cardiovascular comorbidities on senescence, a comorbidity-matched control group was chosen as comparator (Extended Data Table 1). The study was approved by São João Hospital Ethics Committee (ref. 35 – 17), met the ethical standards of the Declaration of Helsinki and donors signed an informed consent according to the Portuguese legislation.

Animal model

Zucker fatty/spontaneously hypertensive heart failure F1 hybrid (ZSF1) Lean (Ln) and Obese (Ob) male rats (Charles River Laboratories) were fed with a standard diet (Purina diet 5008) to develop metabolic syndrome and HFpEF[1]. As previously characterized, both Ln and Ob animals develop hypertension, although only Ob rats develop metabolic syndrome, cardiovascular alterations and exercise intolerance[1,2]. Rats were kept in individually ventilated chambers under controlled environment with a 12-hour light-dark cycle at room temperature (RT). Experimental procedures were carried out in accordance with the Faculty of Medicine of Porto ORBEA guidelines, Portuguese law on animal welfare and EU Directive 2010/63/EU for animal experiments. All protocols and experimental design were approved by Portuguese Veterinary Governmental Authorities (DGAV, 0421/000/000/2013).

Organ collection and blood processing

During sacrifice, organs were weighed, washed in PBS and immediately frozen for subsequent analysis. Blood was collected from subclavian artery in heparinized tubes and centrifuged at 1200 g to isolate plasma and buffy coat. Plasma was then centrifuged for 30 min at 4°C. To isolate peripheral mononuclear cells (PBMCs), buffy coat was overlaid in lymphoprep (Axis-Shield) accordingly to manufacture instructions. Single cell suspensions from the heart were obtained by tissue dissociation with 600 U/mL of collagenase II and 60 U/mL of DNase I using the GentleMACs dissociator (Miltenyi Biotec) as reported elsewhere[43]. Red blood cells (RBCs) were removed from cell suspensions using RBC lysis buffer (Supplementary Table 4).

Senolytic treatment

At the 18th week, ZSF1 Ob rats were randomly allocated to receive 50 mg/Kg/day Nav (Selleckchem; n = 8) or vehicle (10% DMSO + 90 % PEG-300; n = 8) by oral gavage. ZSF1 Lean rats were not exposed to any treatment during the study. Administration followed a 2 cycle-regime of 7 days daily administration, with two weeks of interval. Weight gain was recorded every week along the study and every day prior to administration of Nav (or vehicle). At the 28th week, animals underwent cardiorespiratory capacity evaluation and echocardiography, prior to sacrifice.

Gene expression analysis

RNA was extracted using TRIzol® (Invitrogen) accordingly with manufacturer's instructions. cDNA was synthetized using qScript cDNA Synthesis Kit (Quanta Bio) or PrimeScript RT reagent Kit (Takara) and amplified using SYBR Green technology (NZYSpeedy qPCR Green Master Mix, Nzytech or iQ SYBR Green Supermix, Bio-Rad) on a CFX96™ Real-Time PCR Detection System (Bio-Rad). Primer sequences are available in Supplementary Table 2. Gene expression was normalized to GAPDH or 18s for rat and human samples, respectively. Relative gene expression was based on the ΔΔCq method.

Flow Cytometry

Single-cell suspensions were incubated with anti-rat CD32 in FACS medium during 15 min and subsequently incubated with mix of conjugated antibodies during 20 min, 4 ºC. When apoptosis was evaluated, a subsequent step was performed by incubating cell suspension with annexin-V during 15 min (ThermoFisher). When SA-β-gal was assessed, cells were resuspended in staining medium and the assay was done using Fluorescein di-β-D-galactopyranoside (ThermoFisher), accordingly with manufacturer's instructions. Nonviable cells were detected with 0.5 % propidium iodide (Sigma-Aldrich). For quantitative flow cytometry, precision count beads (Biolegend) were added to cellular suspension (1:4 ratio). Samples were acquired in the cytometer FACS Canto II (BD Biosciences) or in Accuri C6 (BD Biosciences). Data analysis was performed in FlowJo software.

Plasma proteomics

For cytokine and chemokine measurements, plasma-heparin samples from ZSF1 rats with 22 and 26 weeks were analysed at Eve Technologies for the relative quantification of a large array of SASP factors using Rat Cytokine Array/Chemokine Array 27 Plex, RD27.

Immunoblotting

Samples were homogenized in RIPA buffer and protein concentration was quantified using the Bradford assay (Bio-Rad). Proteins (25–60 µg) were separated by sodium dodecyl sulfate-polyacrylamide gel electrophoresis (SDS-PAGE) with a 10–15 % polyacrylamide gel and then electroblotted onto nitrocellulose membranes (Bio-Rad). Blots were blocked in 5 % bovine serum albumin (BSA) in TBS, and then incubated with primary antibodies to BCL-2 (Cell Signaling, #2876), BCL-XL (Cell Signaling, #2764), BAX (Cell Signaling, #2772) and GAPDH (Abcam, #ab8245) in TBS-T (0.1 % Tween-20). Immunoblots were washed and incubated with secondary antibodies coupled to 700 nm or 800 nm infra-red dye in 0.5 % non-fat dry milk in TBS-T. Membrane was washed and imaged with Odyssey Infrared Imaging System (LICOR Biosciences). GAPDH was used as internal control and the control group was set as reference.

Immunofluorescence of tissue sections (IF)

Left ventricle from ZSF1 Lean and Obese rats was collected, fixed in 10 % formalin between 12–24 h and included in paraffin to obtain 4 µm sections. Upon deparaffinization and rehydration, antigen retrieval

(sodium citrate or citrate buffers) was performed and, whenever necessary, slides were permeabilized with 0.1-1 % Triton X-100. Samples were blocked with 5% BSA and incubated with primary antibodies and respective secondary antibodies. Cell nuclei was stained with 4',6'-diamino-2-fenil-indol (DAPI; 5 µg/mL). To decrease autofluorescence, Vector TrueView™ Autofluorescence Quenching Kit (Vector Laboratories) was used.

For isolectin, pH2AX, CD68 immunolabelling, 10 µm or 30 µm cryo-sections from the heart of ZSF1 rats were used. Sections were cut using cryomicrotome (Microtom HM 550, Thermo Scientific), processed and stained as described elsewhere[3]. Nuclei was stained with DAPI (10 µg/mL) and mounted in Fluoroshield mounting media. Images were obtained in a high-content fluorescence microscope (IN Cell 2200) or LSM 710 confocal microscope. Quantifications were performed using ImageJ software.

Immunohistochemistry

Descending aortas from rats were collected, formalin-fixed paraffin-embedded. Sections of 4 µm were used for haematoxylin eosin (H&E), picrosirius red (SR) and Verhoeff–Van Gieson (VVG) staining, according to manufacturer specifications. H&E allowed aortic measurements by defining a region-of-interest. For collagen and elastin quantification, SR or VVG staining's were used, respectively, and a threshold applied to identify collagen or elastin fibers. Elastin fragmentation was defined as the number of visible breaks of continuous elastin fibres. Left ventricle from ZSF1 rats was also collected for detection of collagen content (SR staining). Images were acquired under Zeiss Axio Scan.Z1 slide scanner and quantifications performed with QuPath software.

RNA In Situ Hybridization (RNA-ISH)

RNA-ISH in aortic rings was performed with RNAScope® Multiplex Fluorescent V2 Assay (Advanced Cell Diagnostics), with minor modifications to manufacturer protocol. Images were acquired using confocal microscope (LSM 710). Between 3 to 5 aortic rings were analysed *per* animal. Percentage of $p21^+$ cells was assessed based on the number of cells with ≥ 1 dot/cell. Quantifications were performed in QuPath software.

Endothelial Activation Assay

Human cardiac microvascular endothelial cells (MVECs; #7130, Lonza) were seeded at density of 5000 cells/cm^2 in EGM-2MV microvascular endothelial cell growth medium BulletKit (EGM; Lonza). When cells reached 75–80 % confluency, medium was changed to the following conditions: 1) EBM supplemented with 2 % plasma of rats without lipidic phase; 2) EBM supplemented with 10 % of CM BM-MAC of rats; 3) EBM supplemented with 10 % of plasma of HFpEF or control patients. After 24 h, cells were detached with trypsin/EDTA and MVECs activation was assessed by flow cytometry.

Statistical Analysis

Statistical testing was performed using GraphPad® Prism 8.0 Software. Kolmogorov-Smirnov normality test was used to evaluate normal distribution of data. Normally distributed data was tested with independent sample Student's t test and one-way ANOVA (Bonferroni´s post hoc test) for two or three groups, respectively. Outliers were excluded by ROUT analysis. Non-normally distributed data was tested with Mann-Whitney U test and Kruskal-Wallis one-way ANOVA for two or three groups, respectively. Data with two independent variables were compared with two-way ANOVA followed by pairwise comparison using Bonferroni's post-hoc test. Results are presented as Box Plot with min/max Whiskers or as column bars with Mean ± SEM. Differences between groups were considered significant when $p < 0.05$.

The association between circulating SCs and markers of cardiac overload (BNP and PASP) was assessed using a $\chi 2$ test for linear trend. To optimize the statistical analysis model, variables with skewed distribution, namely BNP, PASP and hsCRP, were transformed to their natural logarithm. A linear regression model was used to assess the association of SC percentage (dependent variable) with biomarkers of inflammation (hsCRP and monocytes), glycemic control (HbA1c) and BMI (independent variables). Statistical analyses were performed with Stata software, version 16.1 SE (StataCorp).

Declarations

Author contributions

DS Nascimento and L Ferreira designed, coordinated the study and participated in the manuscript writing/revision. E Silva and I Tomé were responsible for the collection of biological samples, data acquisition/analysis and drafted the manuscript. F Vasques-Nóvoa and A Leite-Moreira managed the patient cohort and sample collection. A Goncalves, A Silva, V Sampaio-Pinto, D Sousa, C Caetano contributed to data acquisition and analysis. A Barros carried out statistical analyses of clinical data. P Pinto-do-Ó, SG Santos and P Pitrez contributed to data interpretation, design and revisions of data figures. G. Conceição, Nádia, Alexandre, I Falcao-Pires performed physiological and functional tests on animals. All authors participated in discussions and contributed to important advice to the revisions of the manuscript. All authors read and approved the final manuscript.

Competing interests

Andreia Silva is currently an employee of AstraZeneca plc.

Acknowledgements

We thank all the participants for agreeing to join this study. This work was funded by the European Regional Development Fund (ERDF) through COMPETE 2020, Portugal 2020, and by the FCT (Fundação para a Ciência e Tecnologia) [POCI-01-0145-FEDER-016385; POCI-01-0145-FEDER-030985] and by the FCT/Ministério da Ciência, Tecnologia e Inovação in the framework of individual funding

[CEECINST/00091/2018] to DSN, [SFRH/BD/144769/2019] to EDS. The authors acknowledge the support of i3S scientific platforms in particular to Translational Cytometry (TraCy) unit. The authors are thankful to current and past members of each laboratory for critical discussion.

References

1. Shah, K. S. *et al.* Heart Failure With Preserved, Borderline, and Reduced Ejection Fraction. *Journal of the American College of Cardiology* **70**, 2476–2486, doi:doi:10.1016/j.jacc.2017.08.074 (2017).
2. Paulus, W. J. & Tschöpe, C. A novel paradigm for heart failure with preserved ejection fraction: comorbidities drive myocardial dysfunction and remodeling through coronary microvascular endothelial inflammation. *Journal of the American College of Cardiology* **62**, 263–271, doi:10.1016/j.jacc.2013.02.092 (2013).
3. Ridker, P. M. *et al.* Antiinflammatory Therapy with Canakinumab for Atherosclerotic Disease. *New England Journal of Medicine* **377**, 1119–1131, doi:10.1056/NEJMoa1707914 (2017).
4. Tassell, B. W. V. *et al.* IL-1 Blockade in Patients With Heart Failure With Preserved Ejection Fraction. *Circulation: Heart Failure* **11**, e005036, doi:doi:10.1161/CIRCHEARTFAILURE.118.005036 (2018).
5. Minamino, T. *et al.* Ras Induces Vascular Smooth Muscle Cell Senescence and Inflammation in Human Atherosclerosis. *Circulation* **108**, 2264–2269, doi:10.1161/01.CIR.0000093274.82929.22 (2003).
6. Tsuji, T., Aoshiba, K. & Nagai, A. Alveolar Cell Senescence Exacerbates Pulmonary Inflammation in Patients with Chronic Obstructive Pulmonary Disease. *Respiration* **80**, 59–70, doi:10.1159/000268287 (2010).
7. Freund, A., Orjalo, A. V., Desprez, P.-Y. & Campisi, J. Inflammatory networks during cellular senescence: causes and consequences. *Trends in Molecular Medicine* **16**, 238–246, doi:https://doi.org/10.1016/j.molmed.2010.03.003 (2010).
8. Basisty, N. *et al.* A proteomic atlas of senescence-associated secretomes for aging biomarker development. *PLoS biology* **18**, e3000599, doi:10.1371/journal.pbio.3000599 (2020).
9. Nelson, G. *et al.* A senescent cell bystander effect: senescence-induced senescence. *Aging Cell* **11**, 345–349, doi:10.1111/j.1474-9726.2012.00795.x (2012).
10. Ventura, M. T., Casciaro, M., Gangemi, S. & Buquicchio, R. Immunosenescence in aging: between immune cells depletion and cytokines up-regulation. *Clinical and Molecular Allergy* **15**, 21, doi:10.1186/s12948-017-0077-0 (2017).
11. Gevaert, A. B. *et al.* Endothelial Senescence Contributes to Heart Failure With Preserved Ejection Fraction in an Aging Mouse Model. *Circulation. Heart failure* **10**, doi:10.1161/circheartfailure.116.003806 (2017).
12. Jia, K. *et al.* Senolytic Agent Navitoclax Inhibits Angiotensin II-Induced Heart Failure in Mice. *Journal of cardiovascular pharmacology* **76**, 452–460, doi:10.1097/fjc.0000000000000878 (2020).

13. Zhu, Y. *et al.* The Achilles' heel of senescent cells: from transcriptome to senolytic drugs. *Aging Cell* **14**, 644–658, doi:10.1111/acel.12344 (2015).
14. Walaszczyk, A. *et al.* Pharmacological clearance of senescent cells improves survival and recovery in aged mice following acute myocardial infarction. *Aging Cell* **18**, e12945-e12945, doi:10.1111/acel.12945 (2019).
15. Roos, C. M. *et al.* Chronic senolytic treatment alleviates established vasomotor dysfunction in aged or atherosclerotic mice. *Aging Cell* **15**, 973–977, doi:10.1111/acel.12458 (2016).
16. Hamdani, N. *et al.* Myocardial Titin Hypophosphorylation Importantly Contributes to Heart Failure With Preserved Ejection Fraction in a Rat Metabolic Risk Model. *Circulation: Heart Failure* **6**, 1239–1249, doi:doi:10.1161/CIRCHEARTFAILURE.113.000539 (2013).
17. van Dijk, C. G. *et al.* Distinct Endothelial Cell Responses in the Heart and Kidney Microvasculature Characterize the Progression of Heart Failure With Preserved Ejection Fraction in the Obese ZSF1 Rat With Cardiorenal Metabolic Syndrome. *Circulation. Heart failure* **9**, e002760, doi:10.1161/circheartfailure.115.002760 (2016).
18. Abdellatif, M. *et al.* Nicotinamide for the treatment of heart failure with preserved ejection fraction. *Science translational medicine* **13**, doi:10.1126/scitranslmed.abd7064 (2021).
19. Moretta, L. Dissecting CD56dim human NK cells. *Blood* **116**, 3689–3691, doi:10.1182/blood-2010-09-303057 (2010).
20. Franssen, C. *et al.* Myocardial Microvascular Inflammatory Endothelial Activation in Heart Failure With Preserved Ejection Fraction. *JACC. Heart failure* **4**, 312–324, doi:10.1016/j.jchf.2015.10.007 (2016).
21. Boos, C. J., Lip, G. Y. H. & Blann, A. D. Circulating Endothelial Cells in Cardiovascular Disease. *Journal of the American College of Cardiology* **48**, 1538–1547, doi:10.1016/j.jacc.2006.02.078 (2006).
22. Dimri, G. P. *et al.* A biomarker that identifies senescent human cells in culture and in aging skin in vivo. *Proc Natl Acad Sci U S A* **92**, 9363–9367, doi:10.1073/pnas.92.20.9363 (1995).
23. Hamdani, N. *et al.* Myocardial titin hypophosphorylation importantly contributes to heart failure with preserved ejection fraction in a rat metabolic risk model. *Circulation. Heart failure* **6**, 1239–1249, doi:10.1161/circheartfailure.113.000539 (2013).
24. Zile, M. R. *et al.* Prognostic value of brain natriuretic peptide vs history of heart failure hospitalization in a large real-world population. *Clinical Cardiology* **43**, 1501–1510, doi:https://doi.org/10.1002/clc.23468 (2020).
25. Meluzín, J. & Tomandl, J. Can Biomarkers Help to Diagnose Early Heart Failure with Preserved Ejection Fraction? *Disease Markers* 2015, 426045, doi:10.1155/2015/426045 (2015).
26. Pitt, B. *et al.* Spironolactone for Heart Failure with Preserved Ejection Fraction. *New England Journal of Medicine* **370**, 1383–1392, doi:10.1056/NEJMoa1313731 (2014).
27. Borlaug, B. A. *et al.* Effect of Inorganic Nitrite vs Placebo on Exercise Capacity Among Patients With Heart Failure With Preserved Ejection Fraction: The INDIE-HFpEF Randomized Clinical Trial. *JAMA* **320**, 1764–1773, doi:10.1001/jama.2018.14852 (2018).

28. Redfield, M. M. Heart Failure with Preserved Ejection Fraction. *New England Journal of Medicine* **375**, 1868–1877, doi:10.1056/NEJMcp1511175 (2016).
29. Tadic, M. & Cuspidi, C. Obesity and heart failure with preserved ejection fraction: a paradox or something else? *Heart failure reviews* **24**, 379–385, doi:10.1007/s10741-018-09766-x (2019).
30. Glezeva, N. *et al.* Exaggerated inflammation and monocytosis associate with diastolic dysfunction in heart failure with preserved ejection fraction: evidence of M2 macrophage activation in disease pathogenesis. *Journal of cardiac failure* **21**, 167–177, doi:10.1016/j.cardfail.2014.11.004 (2015).
31. Hulsmans, M. *et al.* Cardiac macrophages promote diastolic dysfunction. *Journal of Experimental Medicine* **215**, 423–440, doi:10.1084/jem.20171274 (2018).
32. Zheng, Y. *et al.* A human circulating immune cell landscape in aging and COVID-19. *Protein & Cell* **11**, 740–770, doi:10.1007/s13238-020-00762-2 (2020).
33. Merino, A. *et al.* Senescent CD14 + CD16 + monocytes exhibit proinflammatory and proatherosclerotic activity. *Journal of immunology (Baltimore, Md.: 1950)* **186**, 1809–1815, doi:10.4049/jimmunol.1001866 (2011).
34. Childs, B. G. *et al.* Senescent intimal foam cells are deleterious at all stages of atherosclerosis. *Science* **354**, 472–477, doi:10.1126/science.aaf6659 (2016).
35. Shimizu, I. & Minamino, T. Cellular senescence in cardiac diseases. *Journal of Cardiology* **74**, 313–319, doi:https://doi.org/10.1016/j.jjcc.2019.05.002 (2019).
36. Yousefzadeh, M. J. *et al.* An aged immune system drives senescence and ageing of solid organs. *Nature*, doi:10.1038/s41586-021-03547-7 (2021).
37. Kirkland, J. L., Tchkonia, T., Zhu, Y., Niedernhofer, L. J. & Robbins, P. D. The Clinical Potential of Senolytic Drugs. *Journal of the American Geriatrics Society* **65**, 2297–2301, doi:10.1111/jgs.14969 (2017).
38. Tse, C. *et al.* ABT-263: a potent and orally bioavailable Bcl-2 family inhibitor. *Cancer research* **68**, 3421–3428, doi:10.1158/0008-5472.can-07-5836 (2008).
39. Zhu, Y. *et al.* Identification of a novel senolytic agent, navitoclax, targeting the Bcl-2 family of anti-apoptotic factors. *Aging Cell* **15**, 428–435, doi:10.1111/acel.12445 (2016).
40. Chang, J. *et al.* Clearance of senescent cells by ABT263 rejuvenates aged hematopoietic stem cells in mice. *Nature Medicine* **22**, 78–83, doi:10.1038/nm.4010 (2016).
41. Ponikowski, P. *et al.* 2016 ESC Guidelines for the diagnosis and treatment of acute and chronic heart failure: The Task Force for the diagnosis and treatment of acute and chronic heart failure of the European Society of Cardiology (ESC)Developed with the special contribution of the Heart Failure Association (HFA) of the ESC. *European Heart Journal* **37**, 2129–2200, doi:10.1093/eurheartj/ehw128 (2016).
42. Pieske, B. *et al.* How to diagnose heart failure with preserved ejection fraction: the HFA–PEFF diagnostic algorithm: a consensus recommendation from the Heart Failure Association (HFA) of the European Society of Cardiology (ESC). *European Heart Journal* **40**, 3297–3317, doi:10.1093/eurheartj/ehz641 (2019).

43. Sampaio-Pinto, V. *et al.* Neonatal Apex Resection Triggers Cardiomyocyte Proliferation, Neovascularization and Functional Recovery Despite Local Fibrosis. *Stem Cell Reports* **10**, 860–874, doi:10.1016/j.stemcr.2018.01.042 (2018).

Tables

Table 1. Echocardiography in ZSF1 animals at 28 weeks.

Values are Mean ± SEM (n=8 *per* group). Statistical analysis was done using Kruskal Wallis test with Dunn's correction. *, † are compared to Ln. No statistical significance was found when compared Ln with Ob (Nav) rats. HR - heart rate; dLVPW - left ventricular posterior wall measured in diastole; LV - left ventricular; CI - cardiac index; EF - ejection fraction; E/A - ratio between peak E and A waves of pulsed-wave Doppler mitral flow velocity; E/E' - ratio between peak E wave velocity of pulsed-wave Doppler mitral flow and peak E' wave velocity of tissue Doppler at the lateral mitral annulus; MPI - myocardial performance. Outliers were excluded by ROUT analysis (GraphPad software).

	ZSF1-Ln	**ZSF1-Ob**	**ZSF1-Ob (Nav)**	***p*-value**
				versus Ln
HR (beats per minute)	295.19 ± 7.25	284.50 ± 6.92	272.40 ± 9.84	
LV mass (mg)	1216.94 ± 38.84	1573.79 ± 28.84*	1564.47 ± 32.06†	* p=0.002 † p=0.002
CL (μL/min/cm^2)	44.82 ± 4.79	57.72 ± 4.03	66.11 ± 4.99	
EF (%)	68.71 ± 1.57	71.80 ± 1.08	72.04 ± 1.91	
E/A	2.04 ± 0.22	1.39 ± 0.06*	1.42 ± 0.08	* p=0.04
E/E'	14.44 ± 0.47	17.70 ± 1.33	18.39 ± 0.93†	† p=0.01
MPI (Tei index)	0.53 ± 0.02	0.52 ± 0.02	0.51 ± 0.02	

Extended Data Table 1: Characteristics of Patient Population

Plus-minus values are mean ± SEM. IQR – interquartile range. 2-tailed t-test and Mann-Whitney test were used for variables with normal and non-normal distribution respectively. **CM-Ctrl** - comorbidity-matched

control group; **HFpEF** – heart failure with preserved ejection fraction. BMI – body-mass index; NYHA – New York Heart Association; ECW – extracellular water; TBW – total body water, LVEF – left ventricular ejection fraction; LAVI – left atrial volume index; LVMI – left ventricle mass index; PASP – pulmonary artery systolic pressure; eGFR – estimated glomerular filtration rate; HbA1c – glycated hemoglobin; hsCRP – high-sensitivity C-reactive protein; hsTnI – high-sensitivity troponin I; BNP – B-type natriuretic peptide; ACEi/ARB – angiotensin-converting enzyme inhibitors/angiotensin receptor blockers.

Characteristic	CM-Ctrl (n=10)	HFpEF (n=46)	*p-value*
Median Age – years (IQR)	64 (57-73)	72 (66-79)	NS
Male sex – no. (%)	6 (60.0)	27 (58.7)	NS
BMI – Kg/m^2	30.5 ± 1.4	29.1 ± 0.7	NS
Cardiovascular Comorbidities			
Hypertension – no. (%)	8 (80.0)	44 (95.6)	NS
Diabetes – no. (%)	6 (60.0)	26 (56.2)	NS
Dyslipidemia – no. (%)	9 (90.0)	41 (89.1)	NS
Smoking – no. (%)	5 (50.0)	17 (36.9)	NS
Atrial Fibrillation – no. (%)	0 (0.0)	16 (34.8)	**0.03**
HF Signs and Symptoms			
Lung Congestion – no. (%)	2 (20.0)	27 (58.7)	**0.03**
Peripheral edema – no. (%)	2 (20.0)	33 (71.7)	**0.002**
NYHA functional classification – no. (%)			
I	-	19 (41.3)	-
II	-	23 (50.0)	-
III	-	4 (8.7)	-
Bioimpedance			
Median ECW/TBW - % (IQR)	38.1 (37.5-38.9)	39.4 (38.5-40.1)	**0.05**
Echocardiographic evaluation			
LVEF - (%)	62.8 ± 0.9	62.3 ± 0.6	NS
LAVI – (mL/m^2)	26.5 ± 1.9	36.6 ± 1.3	**0.002**
LVMI – (g/m^2)	126.7 ± 9.6	140.6 ± 4.2	NS

E/E’	8.1 ± 0.8	9.9 ± 0.4	NS
PASP – mmHg (IQR)	24 (21-29)	30 (25-40)	**0.05**
Analytical Evaluation			
Hemoglobin - g/dL	13.5 ± 0.5	12.6 ± 0.3	NS
Median eGFR - mL/min/1.73m^2	93.9 (82.6-109.8)	82.5 (49.8-112.9)	NS
Total Cholesterol - mg/dL	156.4 ± 11.6	145.2 ± 6.5	NS
Apolipoprotein B - mg/dL	81.0 ± 6.5	77.0 ± 2.9	NS
Median HbA1c - % (IQR)	6.2 (5.6-7.4)	6.1 (5.5-6.9)	NS
Median hsCRP - mg/L (IQR)	2.8 (1.1-4.6)	2.6 (0.7-6.4)	NS
Median hsTnI - pg/L (IQR)	3.1 (1.9-3.7)	6.6 (3.9-10.2)	**0.003**
Median BNP -pg/mL (IQR)	25.6 (17.2-37.7)	110 (80.1-210.8)	**<0.001**
Medication			
Beta-blocker – no. (%)	2 (20.0)	31 (67.4)	**0.01**
Loop Diuretics – no. (%)	1 (10.0)	31 (67.4)	**0.002**
ACEi/ARB – no. (%)	6 (60.0)	28 (60.9)	NS
Statin – no. (%)	6 (60.0)	37 (80.4)	NS

Extended Data Table 2: Morphometric data, exercise tolerance tests and metabolic assessment in ZSF1 animals at 28 weeks. Data are Mean ± SEM (n=8 *per* group). Statistical significance was evaluated by Kruskal-Wallis test with Dunn’s *post hoc* correction. *ZSF1-Ln vs. ZSF1-Ob and †ZSF1-Ln vs. ZSF1-Ob (Nav). No statistical significance was found when compared Ln with Ob (Nav) rats. TL - tibia length; RK - right kidney; LK - left kidney; VO_2 max - maximal oxygen consumption; VCO_2 max - maximal carbon oxide output.

	ZSF1-Ln	ZSF1-Ob	ZSF1-Ob (Nav)	*p*-value versus Ln
Morphometric parameters				
Tibia length (cm)	4.38 ± 0.03	4.07 ± 0.05*	4.11 ± 0.02†	* p=0.001 † p=0.003
Body weight (mg/cm)	514.00 ± 5.95	693.75 ± 15.42*	667.50 ± 18.96†	* p=0.006 † p=0.02
Lung weight/TL (mg/cm)	378.11 ± 16.90	431.34 ± 19.88	394.43 ± 11.71	
Spleen weight/TL (mg/cm)	160.58 ± 1.20	227.05 ± 7.32 *	203.38 ± 8.21†	* p=0.0001 † p=0.02
Liver weight/TL (mg/cm)	3503.83 ± 108.05	1898.91 ± 671.37*	10077.01 ± 261.72†	* p=0.001 † p=0.003
Right kidney weight/TL (mg/cm)	386.02 ± 8.36	633.98 ± 31.02*	556.14 ± 19.18†	* p=0.0003 † p=0.01
Left kidney weight/TL (mg/cm)	393.07 ± 9.03	622.93 ± 34.92*	553.21 ± 19.21†	* p=0.0003 † p=0.01
Gastrocnemius weight/TL (mg/cm)	627.90 ± 8.36	493.20 ± 15.49*	450.78 ± 14.26†	* p=0.01 † p=0.0002
Soleus weight/TL (mg/cm)	57.43 ± 1.19	51.93 ± 0.69*	51.38 ± 1.05†	* p=0.007 † p=0.01
Perigonadal fat weight/TL (mg/cm)	757.24 ± 28.22	1280.18 ± 30.40*	1320.64 ± 101.67†	* p=0.07 † p=0.003
Perirenal fat weight/TL (mg/cm)	846.95 ± 54.29	6439.88 ± 190.30*	5268.27 ± 403.30†	* p<0.0001 † p=0.003
Visceral fat weight/TL (mg/cm)	1017.48 ± 59.71	2577.65 ± 105.21*	2625.28 ± 144.32†	* p=0.006 † p=0.002
Performance test				
VO_2max (mL/min/$Kg^{0.75}$)	33.99 ± 0.71	15.31 ± 0.12*	18.67 ± 1.41†	* p=0.0002 † p=0.02

VCO_2max (mL/min/$Kg^{0.75}$)	31.57 ± 0.75	16.68 ± 0.07*	20.10 ± 1.18†	* p=0.0002 † p=0.02
Respiratory exchange ratio	0.93 ± 0.01	1.10 ± 0.64*	1.09 ± 0.02†	* p=0.001 † p=0.004
Metabolism and renal function				
Glucose (mg/dL)	191.63 ± 13.53	279.48 ± 20.72*	258.17 ± 4.14	* p=0.009
Total cholesterol (mg/dL)	82.00 ± 3.70	284.86 ± 12.86*	259.29 ± 11.01†	* p=0.0008 † p=0.01
Triglycerides (mg/dL)	100.38 ± 9.16	1322.86 ± 93.86*	1523.29 ± 60.31†	* p=0.02 † p=0.0003
Urea (mg/dL)	28.21 ± 1.05	45.16 ± 1.02*	40.46 ± 3.06†	* p=0.002 † p=0.01
Creatinine (mg/dL)	0.46 ± 0.02	0.31 ± 0.02*	0.30 ± 0.00†	* p=0.003 † p=0.002

Figures

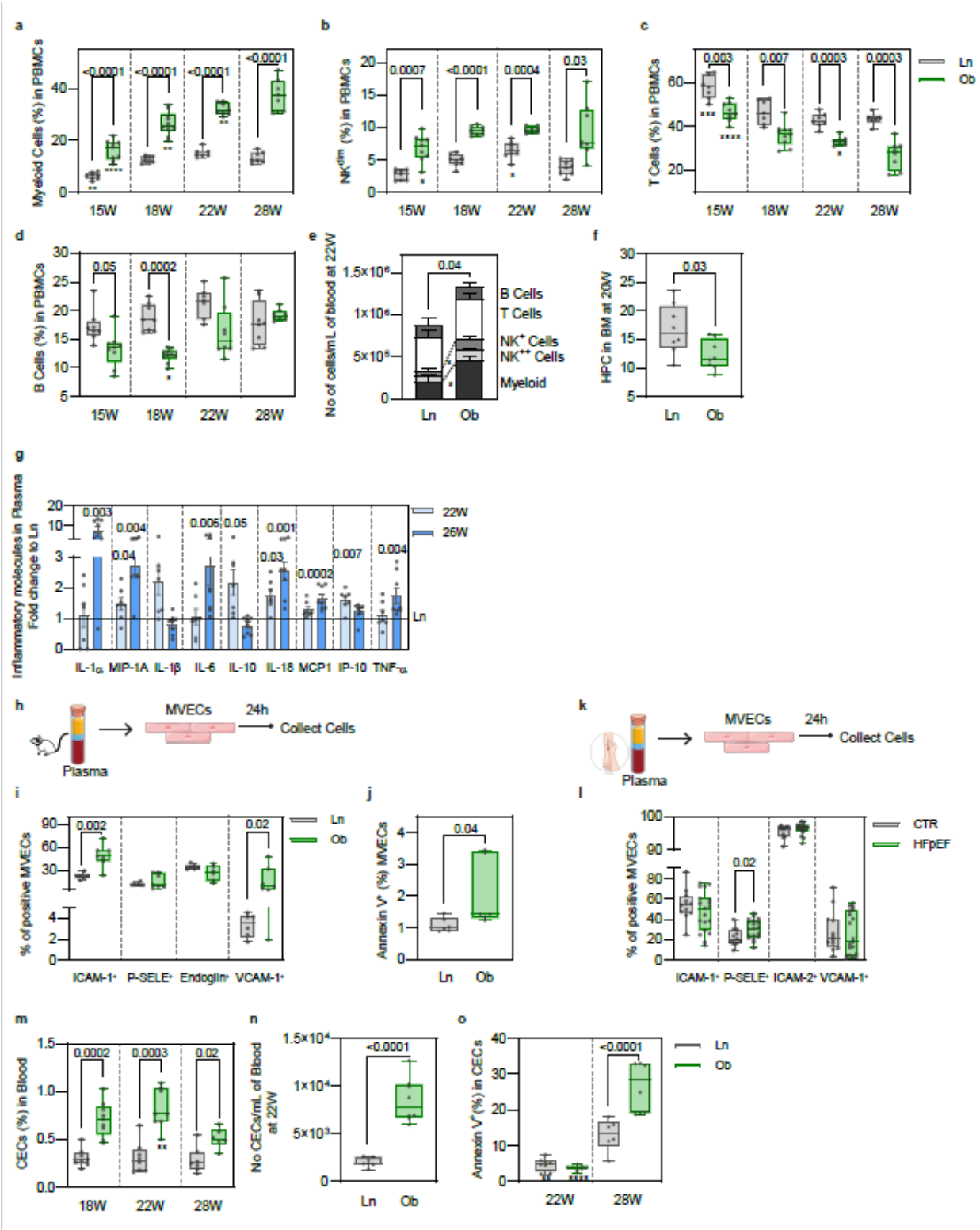

Figure 1

ZSF1-Obese rats show alterations in the immune system, inflammaging and endothelial dysfunction. a. Relative percentage of myeloid cells (TCR- CD45R- CD161a- CD11bc+), b. NKdim cells (TCR-CD161adim), c. T cells (TCR+CD161a-) and d. B cells (CD45R+) in peripheral blood mononuclear cells (PBMCs) isolated at 15, 18, 22 and 28 weeks from ZSF1-obese (Ob) and control ZSF1-Lean (Ln) rats (n=7/group). e. Absolute numbers of PBMCs and of each immune population per mL of blood at 22 weeks in Ln and

Ob rats (n=8/group). f. Relative percentage of hematopoietic progenitors (HPC) (CD45+CD45R-TCR-CD161a-CD11bc-) in bone marrow at 20 weeks in Ln and Ob rats (n=8/group). g. Profiling of inflammatory molecules in plasma of Ob and Ln rats with 22 and 26 weeks (n=7/group). Protein levels in ZSF1-Ob were normalized to Ln. h. Human microvascular endothelial cells (MVECs) were exposed to plasma of Ln and Ob rats (n=6/group) and k. plasma of HFpEF (n=19) and control (CTR) patients (n=12) for 24 hours. i. and l. Percentage of MVECs activation and j. apoptosis was assessed by surface expression of adhesion molecules and detection of annexin V. m. Proportion of circulating endothelial cells (CECs) (CD31+CD45-) in PBMCs at 18, 22 and 28 weeks of Ln and Ob (n>5/group). n. Absolute numbers of CECs per mL of blood at 22 weeks of Ln and Ob rats (n=8/group). o. Apoptotic cells (Annexin V+) in the circulating endothelial cell compartment at 22 (n>7/group) and 28 (n>5/group) weeks. All values are presented as box and whiskers plots with min to max values, except on e. and g. in which values are presented as mean ± SEM. P-values above data refer to the comparison of Ln versus Ob at a specific time point and symbols below the data report on differences to the following time-point (* (p≤ 0.05), ** (p≤ 0.01), *** (p≤ 0.001) and **** (p≤ 0.0001)).

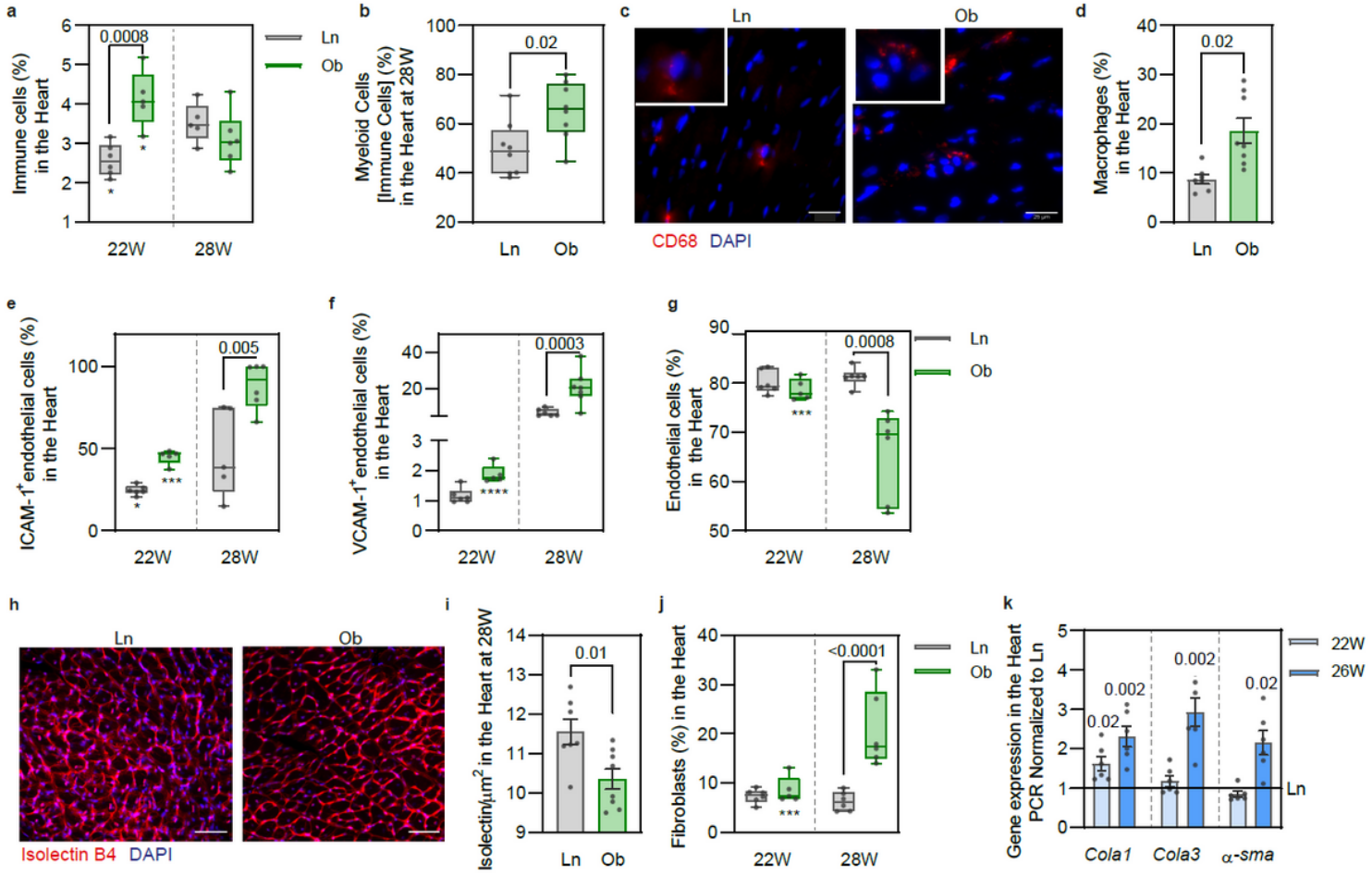

Figure 2

ZSF1-Obese hearts show infiltration of immune cells, endothelial dysfunction and fibrosis. a. Immune infiltrate (CD45+) in the myocardium. b. Percentage of myeloid cells (CD11bc+) from total immune cells infiltrating the myocardium at 28 weeks (n=8/group). c. Representative images and d. respective

quantification of macrophages (CD68; red) in the Ln and Ob heart at 28 weeks (n=8/group). Scale bars 25 µm. e. Percentage of cardiac endothelial cells (CD31+CD45-) expressing the adhesion molecules ICAM-1 and f. VCAM-1 at 22 and 28 weeks of life (n=8/group). g. Percentage of endothelial cells of total cardiac cells isolated at 22 and 28 weeks (n=7/group). h. Representative confocal images and i. respective quantification of the myocardial endothelial network (Isolectin B4; red) in the Ln and Ob at 28 weeks (n=7/group). Scale bars 25 µm. j. Percentage of fibroblasts (CD45-CD31-PDGFRα+) of total isolated heart cells at 22 and 28 weeks (n=7/group). k. Expression of fibroblast activation-associated genes in the myocardium at 22 and 28 weeks (n≥5/group) presented as ratio to the levels of Ln rats. The values are presented as mean ± SEM on d., i. and k., or as box and whiskers with min to max values. P-values above data to compare Ln versus Ob at a specific time point and symbols below the data to compare Ln and Ob at different time points (* (p≤ 0.05), ** (p≤ 0.01), *** (p≤ 0.001) and **** (p≤ 0.0001)).

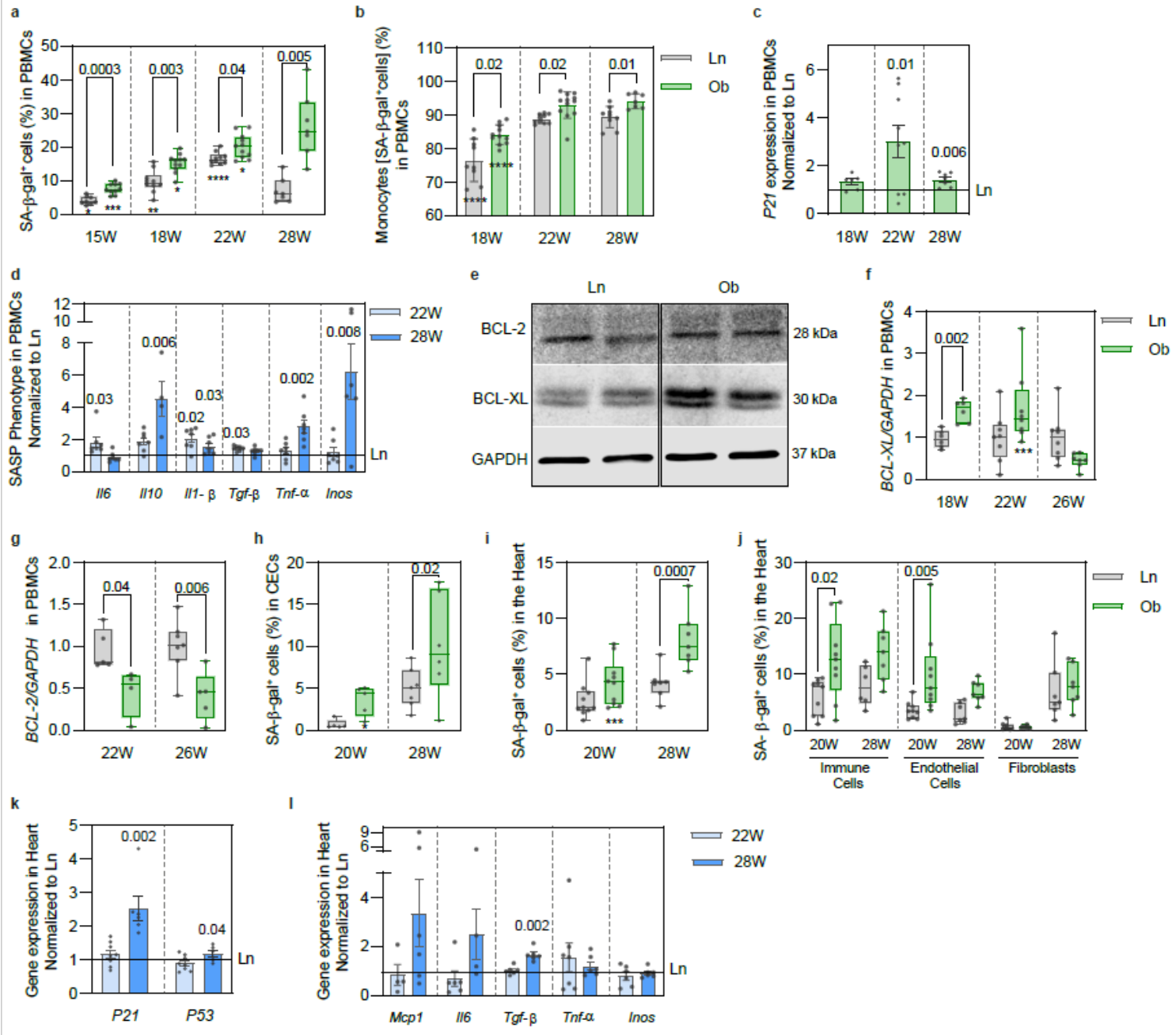

Figure 3

Evidence of premature cell senescence in ZSF1-Ob rats. a. Immunosenescence. Relative percentage of senescent-associated beta-galactosidase-expressing cells (SA-β-gal) in PBMCs and b. monocytes within the SA-β-gal+ subset at 15, 18, 22 and 28 weeks in Ln and Ob rats (n=7/group). c. Transcriptomic profiling of PBMCs for p21 and d. the senescent associated phenotype (SASP) from 18 to 28 weeks (n ≥ 6/group). Ob expression levels were normalized to Ln. e-g. Measurement of BCL-XL and BCL-2 pro-survival molecules in PBMCs lysates at 18, 22 and 28 weeks by western blot (n≥4/group). Data presented as the ratio with GAPDH. h. SA-β-gal positive CECs in blood at weeks 20 and 28 (n≥5/group). i. Myocardial senescence. Percentage of SA-β-gal positive cells in heart and in j. non-cardiomyocyte populations at 20 and 28 weeks in Ln and Ob rats (n ≥ 7/group). k. Transcriptomic profiling of the heart of Ob rats for senescence markers, p21 and p53, and l. SASP levels at 22 and 28 weeks (n≥5/group), presented as a fold change relative to Ln. The values are presented as mean ± SEM or as box and whiskers with min to max values. P-values above data to compare Ln versus Ob at a specific time point and symbols below the data to compare Ln and Ob at different time points (* (p≤ 0.05), ** (p≤ 0.01), *** (p≤ 0.001) and **** (p≤ 0.0001)).

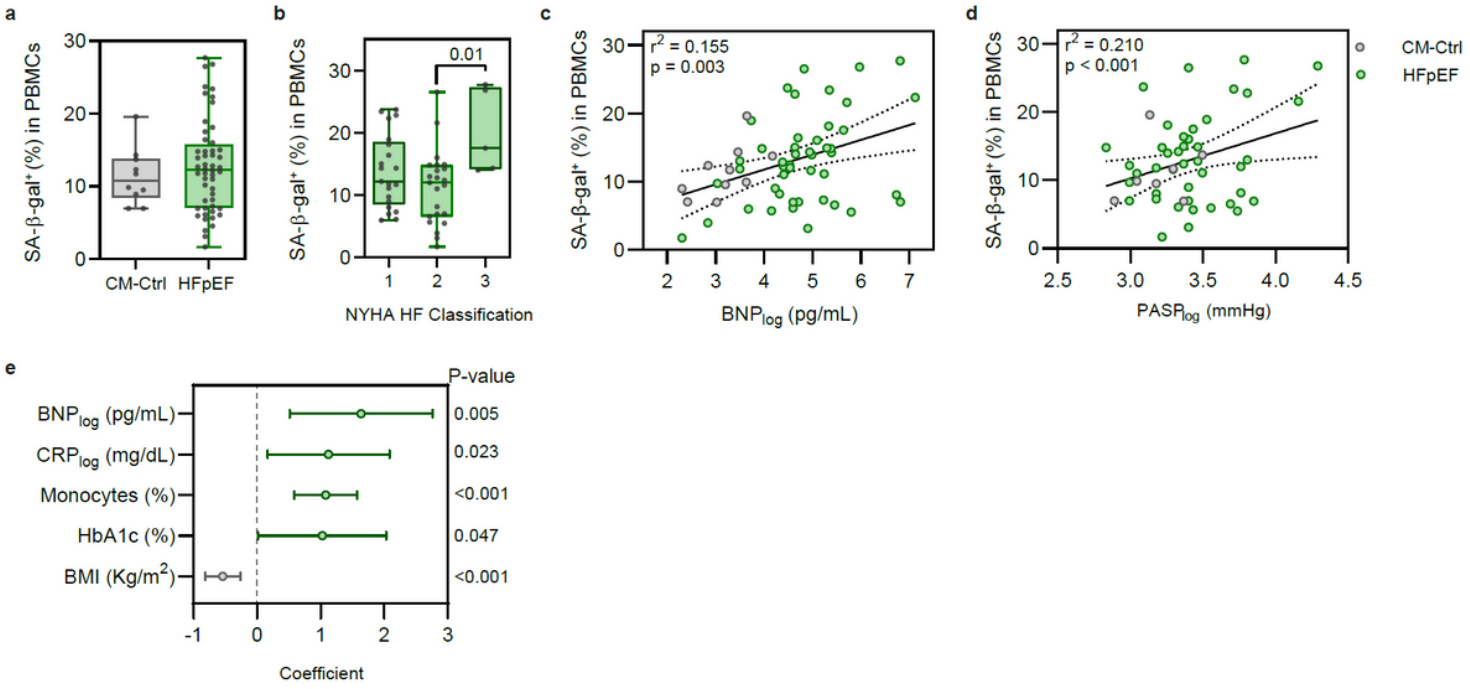

Figure 4

Cell senescence correlate with markers of cardiac overload and systolic pressure in pulmonary artery a. Relative percentage of SA-β-gal+ in PBMCs in CM-Ctrl (n=10) and HFpEF (n=46) groups and b. according to the New York Heart Association functional classification in HFpEF (NYHA HF). c. Association between SA-β-gal+ and key analytical BNPlog and d. clinical PASPlog surrogates of cardiac overload and prognosticators in HFpEF. e. Forest plot depicting correlation coefficients and confidence intervals (multiple linear regression model) assessing the between major risk factors/prognosticators in HFpEF and circulating SCs. The values are presented as box and whiskers with min to max values. BNPlog – B-

type natriuretic peptide, log-transformed; PASPlog – pulmonary artery systolic pressure, log-transformed; hsCRPlog – high-sensitivity C-reactive protein, log-transformed; HbA1c – glycated hemoglobin; BMI – body mass index.

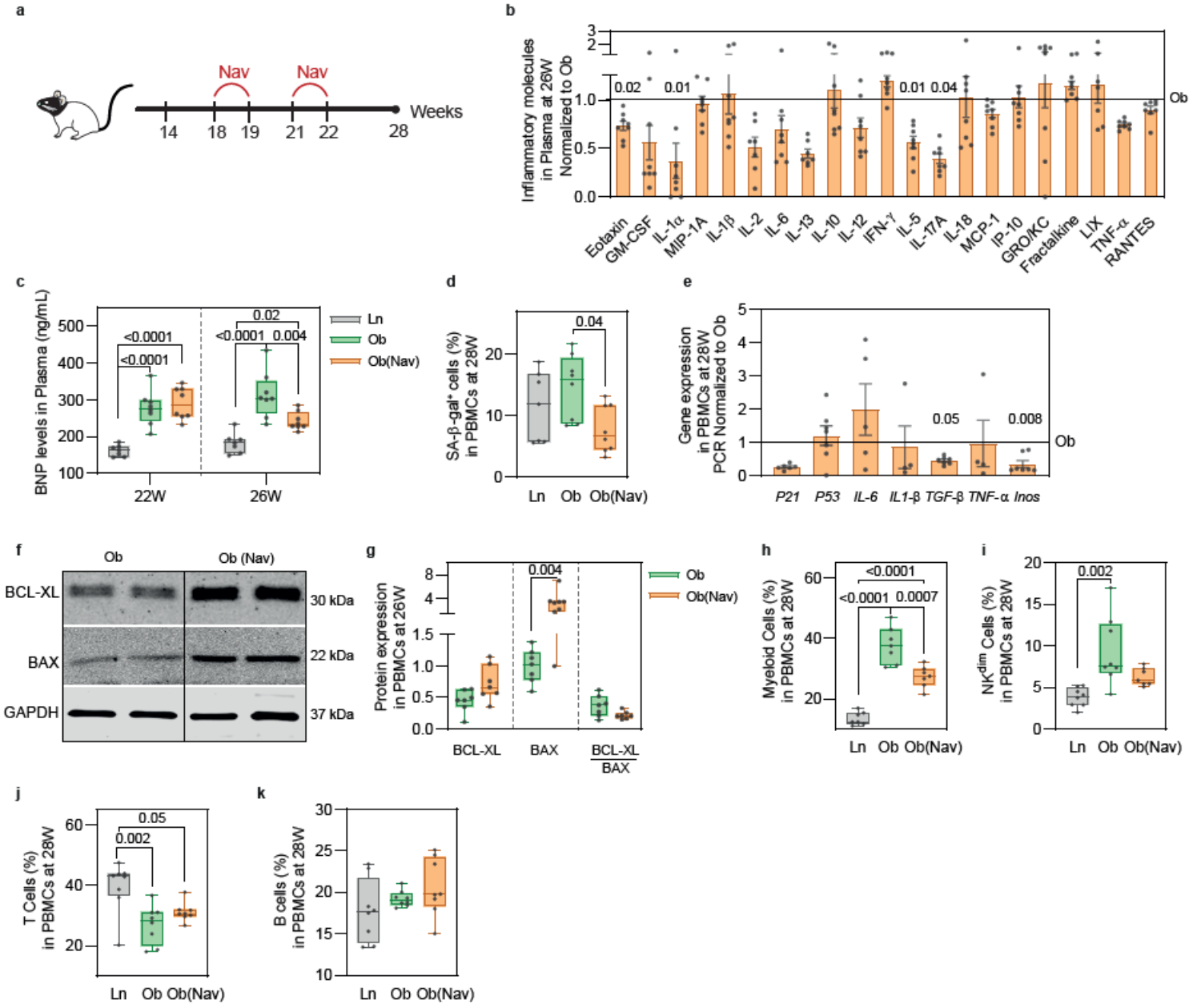

Figure 5

Nav-treated ZSF1-Ob rats display lower levels of circulating BNP levels, inflammation and immunosenescence. a. Schematic representation of Nav administration in Ob rats (n=8/group). Administration followed a 2 cycle-regime of 7 days daily administration, with two weeks of interval. b. Profiling of inflammatory molecules in plasma of Ob (Nav) rats with 26 weeks (n=7/group), normalized to Ob levels. c. Levels of circulating BNP in plasma of Ln, Ob and Ob (Nav) with 22 and 26 weeks. Data was normalized with previous values of the respective animal. d. Frequency of SA-β-gal+ cells in PBMCs at 28 weeks in Ln, Ob and Ob (Nav) rats (n=7/group). e. Transcriptomic profiling of PBMCs for p21, p53 and senescent associated phenotype (SASP) genes at 28 weeks on Ob (Nav) (n ≥ 6/group). Expression levels

were normalized against GAPDH and presented as ratio to the levels of Ob rats. f-g. Quantification of BCL family members, BCL-XL and BAK, in PBMCs at 28 weeks by western blot (n≥6/group). Data presented as the ratio to GAPDH. h. Relative percentage of myeloid cells (TCR- CD45R- CD161a- CD11BC+), i. NKdim cells (TCR-CD161adim), j. T cells (TCR+) and k. B cells (CD45R+) in PBMCs at 28 weeks in Ln, Ob and Ob (Nav) rats (n≥7/group). Values are presented as mean ± SEM or as box and whiskers with min to max values.

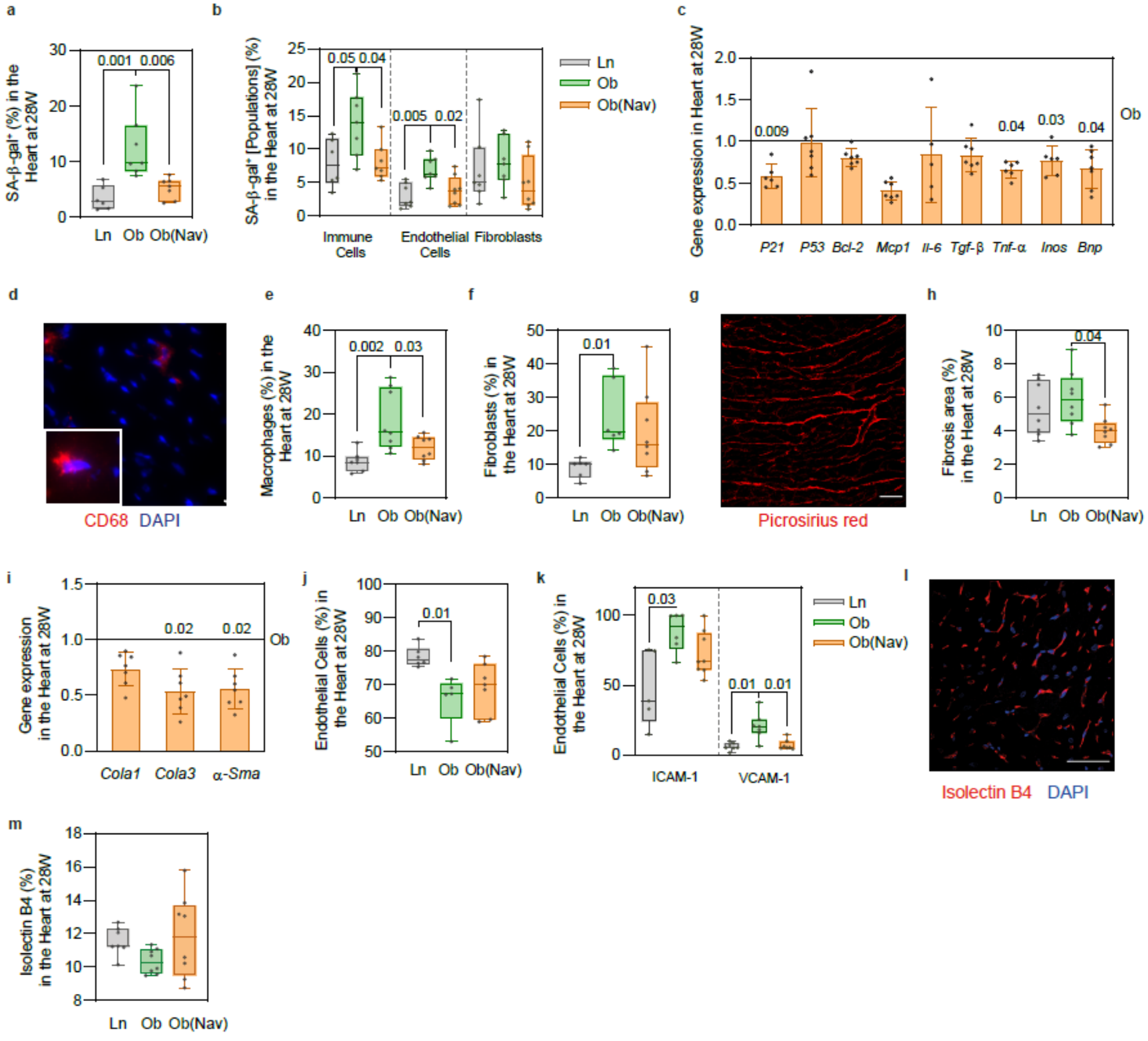

Figure 6

Treatment of ZSF1-Ob rats with Nav decreased heart cell senescence, fibrosis and endothelial dysfunction. a. Percentage of SA-β-gal+ cells in the heart and b. in different non- cardiomyocyte populations from Ln, Ob and Ob (Nav) rats with 28 weeks (n ≥ 7/group). c. Transcriptomic profile of the

heart for senescence markers, SASP and BNP at 28 weeks (n ≥ 6/group), presented as a fold change relative to Ob rats. d. Representative images and e. respective quantification of macrophages (CD68; red) in Ln, Ob and Ob (Nav) hearts at 28 weeks (n=8/group). Scale bars 25 μm. f. Percentage of fibroblasts (CD45-CD31-PDGFRα+) in the heart at 28 weeks (n ≥ 6/group). g. Representative images and h. respective quantification of picrosirius red at 28 weeks (n=8/group). Scale bars 50 μm. i. Expression of fibroblast activation-associated genes in the myocardium at 28 weeks (n=5/group) presented as ratio to the levels of Ob rats. j. Percentage of endothelial cells (CD31+CD45-) of total cardiac cells isolated at 28 weeks (n=7/group). k. Percentage of cardiac endothelial cells expressing ICAM-1 and VCAM-1 (n ≥ 6/group). l. Representative images and m. respective quantification of Isolectin B4 (red) staining in the heart at 28 weeks. Scale bar 50 μm. Values are presented as mean ± SEM or as box and whiskers with min to max values.

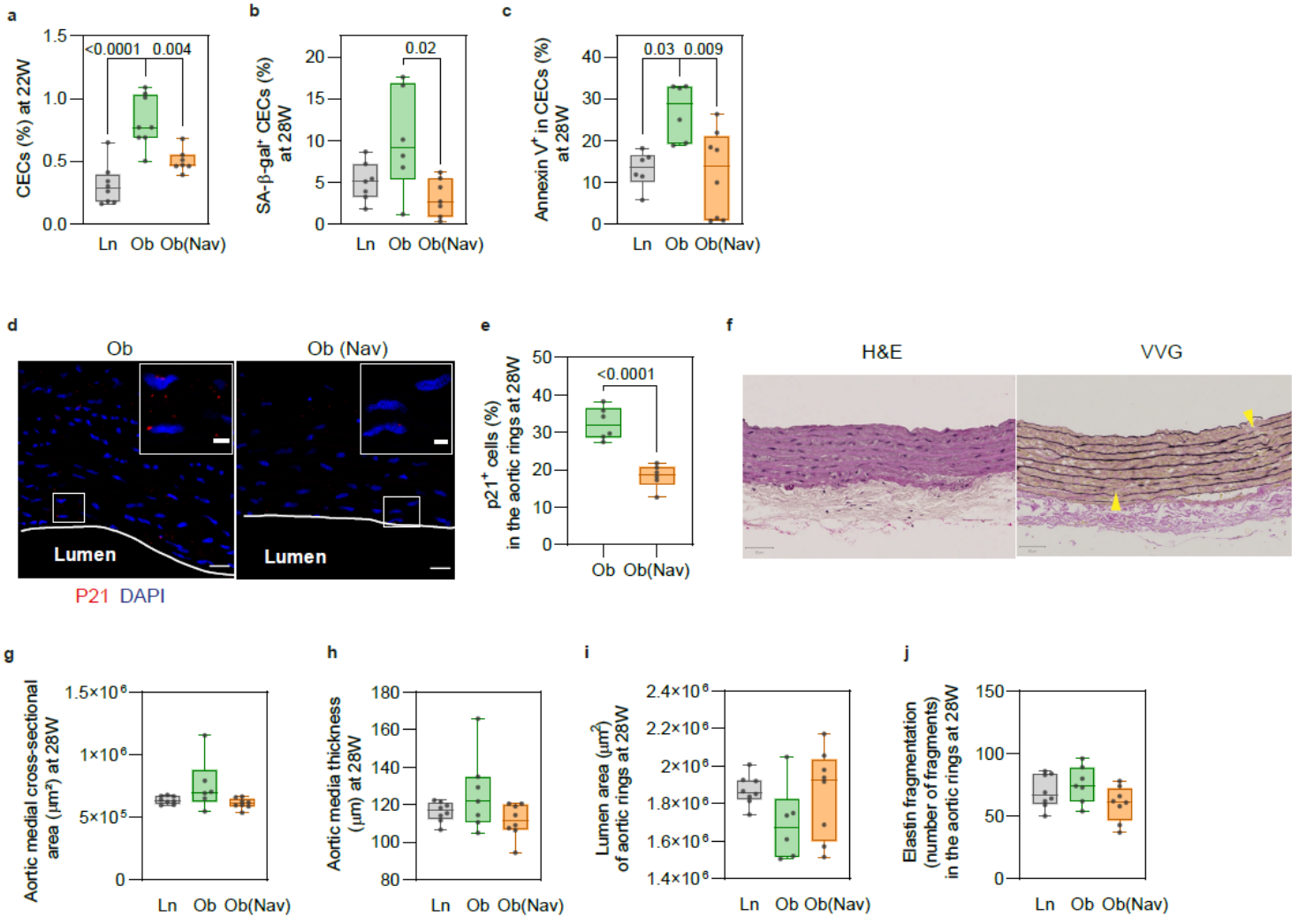

Figure 7

Treatment of ZSF1-Ob rats with Nav decreased circulating endothelial cells, vascular cell senescence and hypertrophy. a. Proportion of circulating endothelial cells (CECs; CD31+CD45-) at 22 weeks (n > 7/group). b. Percentage of SA-β-gal+ cells in CECs at 28 weeks (n > 7/group). c. Apoptotic cells (Annexin V+) in CECs at 28 weeks (n>7/group). d. Representative images and e. respective quantification of IHC RNA-ISH

staining for p21 (red) at 28 weeks in aortic rings (n=6/group). Scale bar 20 μm. f. Representative images of aortic wall sections stained with haematoxylin eosin (H&E) and Verhoeff's Van Gieson (VVG). Scale bar 50 μm. g-i. Quantification of morphological parameters of the aortic wall by H&E. Region-of-interest was defined in the media aortic wall (continuous red line) of the lumen (n>7/group). j. Quantification of elastin fragmentation in the aortic wall (yellow arrows) (n>7/group). Values are presented as box and whiskers with min to max values.

Supplementary Files

This is a list of supplementary files associated with this preprint. Click to download.

- ExtendedData1.pdf
- ExtendedData2.pdf
- ExtendedData3.pdf
- ExtendedData4.pdf
- ExtendedData5.pdf
- SupplementaryMethods.docx